Delft University of Technology

Climate Assessment of Hydrogen Combustion Aircraft: Towards a Green Aviation Sector

Saez Ortuño, M.A.; Yin, F.; Gangoli Rao, A.; Vos, Roelof; Proesmans, P.

Important note
To cite this publication, please use the final published version (if applicable).
Please check the document version above.

Climate Assessment of Hydrogen Combustion Aircraft: Towards a Green Aviation Sector

Miguel Sáez Ortuño[1], Feijia Yin[2], Arvind Gangoli Rao[3], Roelof Vos[4] and Pieter-Jan Proesmans[5]
Delft University of Technology, Kluyverweg 1, 2629HS, Delft, the Netherlands, The Netherlands

As climate change aggravates, the aviation sector strives to minimize its climate footprint. To this end, international organizations, such as ICAO and ACARE, are promoting mitigation measures including novel technologies, operations, and energy carriers to reduce aircraft emissions significantly. Hydrogen (H_2) as an alternative fuel has the advantage of eliminating CO_2 and soot emissions and the potential to reduce NO_x emission substantially. Nevertheless, burning H_2 emits more H_2O and increases the contrail formation probability. Therefore, the actual climate impact of hydrogen aircraft is still uncertain. This paper intents to evaluate the climate impact of a hydrogen powered aircraft considering the effects of H_2O, NO_x, and contrails . To frame the contribution of each individual climate agent, the research compares a hydrogen and a kerosene aircraft with similar mission capabilities. To assess the climate impact, a modeling chain was developed including network selection, flight routes calculation, aircraft and propulsion performance, emissions prediction, and climate impact assessment. In total, 2.24 million flights covering 1128 city pairs were analyzed. The energy consumption of hydrogen aircraft is about 10% higher than that of the kerosene aircraft due to the larger wetted area for hydrogen storage. However, the average atmospheric temperature response caused by the hydrogen aircraft is 67% lower compared to the kerosene aircraft due to the absence of CO_2, the lower radiative forcing of hydrogen contrails, and the reduction in NO_x emissions when assuming advanced hydrogen combustion technology. It was also observed that climate impact from hydrogen aircraft is more sensitive to flights over the tropics than to flights over the poles.

Nomenclature

Latin Symbols

$C_{D,0}$	Zero-Lift Drag Coefficient [-]
c_P	Constant Pressure Specific Heat [kJ/kgK]
D	Drag [N]
h	Altitude [m]
k	Lift-Induced Drag Coefficient Factor [-]
L	Lift [N]
l	Cabin Length [m]
$\dot{m}$	Mass Flow [kg/s]
P	Ambient Pressure [Pa]
P_{t_3}	Pressure Combustion Chamber [Pa]
p_3	Pressure Combustion Chamber [psia]
Q	Fuel Specific Heat [kJ/kg]
R	Range [km]
T	Thrust [N]
T_{t_3}	Temperature Combustion Chamber [K]
t	time [s]
W	Weight [N]

$W_{f,c}$	Weight Fuel Contingency [N]
$W_{f,rec,c}$	Weight Required Fuel Contingency [N]
$W_{f,used}$	Weight Fuel Used [N]
S	Wing Area [m^2]
V	Flight Velocity [m/s]

Greek Symbols

η	Overall Propulsion Efficiency [-]
ϵ	Ratio of the molar masses of water and air [-]
γ	Flight Path Angle [deg]

Acronyms

ATR	Average Temperature Response
BAU	Business As Usual
CO_2	Carbon Dioxide
EI	Emission Index
ERF	Effective Radiative Forcing
FZM1G	Fly-Zero Midsize Segment Aircraft

---

[1]MSc Student, Flight Performance and Propulsion, miansaor@gmail.com, AIAA Student Member.

[2]Assistant Professor, corresponding author, Aircraft Noise and Climate Effects, f.yin@tudelft.nl, AIAA member.

[3]Full Professor, Flight Performance and Propulsion, a.gangolirao@tudelft.nl, AIAA member.

[4]Associate Professor, Flight Performance and Propulsion, r.vos@tudelft.nl, AIAA Associate member.

[5]PhD Candidate, Flight Performance and Propulsion, p.proesmans@tudelft.nl, AIAA Student Member.

GHG	Greenhouse Gas	O_2	Oxygen
H_2	Hydrogen	OEW	Operative Empty Weight
H_2O	Water Vapour	PRC	Payload Range Capacity
KER	Kerosene	RF	Radiative Forcing
N_2	Nitrogen	ROC	Rate of Climb
NO_x	Nitrogen Oxide	ROD	Rate of Descent
MTOW	Maximum Take Off Weight	SAC	Schmidt-Appleman Criterion
LHV	Lower Heating Value		

I. Introduction

As climate change aggravates, international institutions, nations and companies strive to reduce greenhouse gas (GHG) emissions in all economic sectors. Aviation is one of the few industries whose emissions are released both at the Earth's surface and in the upper troposphere and lower stratosphere. In 2019, aviation contributed to 12% of the total GHG emissions from the transport sector and 2.1% of the total anthropogenic emissions [1]. In terms of climate impact, aviation contributes to approximately 4% of the total anthropogenic radiative forcing (RF) including both CO_2 and non-CO_2 effects [1]. The non-CO_2 effects include nitrogen oxide (NO_x) induced ozone (O_3) formation, water vapor (H_2O), and contrail/contrail-cirrus, whose climate impact at higher altitudes is as important as CO_2 [1, 2]. The fragility of the climate with respect to high-altitude emissions drives the aerospace industry to drastically reduce its emissions via improved technology (e.g.,aerodynamic and propulsion) and changes in fleet operations [3]. However, research [4] has shown that these proposals are not sufficient to fight climate change and meet the 2.0ºC maximum increase proposed by the Paris Agreement, as demand for air transport is expected to increase exponentially in the coming decades[2]. Consequently, the aerospace sector needs revolutionary designs and technological combinations [5]. This is where the use of alternative energy carriers, such as hydrogen, could intervene.

The emission characteristics of hydrogen (H_2) combustion differ significantly from kerosene combustion. While burning H_2 eliminates carbon emissions (e.g., CO_2 and non-volatile matters (nvPM)), it increases H_2O emissions by 2.6 times per unit energy. H_2O is a direct GHG emission and the residence time increases as the emission altitude increases, which implies a stronger climate impact from H_2O emissions [6]. Furthermore, H_2O emission is strongly related to persistent contrail formation, which is one of the largest climate agents for aviation [7] (also see details in Sec. II of this paper). Hydrogen combustion tends to form more NO_x due to its higher flame temperature than kerosene combustion unless a lean combustion mode is applied [8]. From an aircraft design perspective, previous studies demonstrated that hydrogen-powered aircraft are less energy efficient [5, 9]. This is mainly because carrying hydrogen on-board requires more volume, which increases the wetted area of the airframe, hence penalizing the aerodynamic performance.

Given to the pros and cons mentioned above, the total climate impact of hydrogen aircraft is rather ambiguous. Therefore, the objective of this study is to quantify the total climate impact caused by a fleet of both hydrogen and kerosene combustion aircraft using a newly established in-house model chain. We investigate three aspects: 1) the changes of climate impact from individual species when switching from kerosene to hydrogen aircraft, 2) the geographical effects of the emissions, i.e., how emissions affect the climate at different latitudes and altitudes; 3) sensitivity of the results with respect to various uncertainty sources, including the variability of the NO_x emissions index, the radiative forcing of contrails from hydrogen aircraft, and the flight altitude.

The paper is structured as follows. Sec. II introduces prerequisite knowledge that is relevant to this study. The modelling chain, including various submodules, to solve the objective of the study are elaborated in Sec. III. Sec. IV focuses on the results of the study including the design details of the fleets involved, the routes selected, the total calculated emissions and finally the change of atmospheric temperature concerning different fleets. To ultimately assess whether the hydrogen aircraft is a superior option to fight climate change, a sensitivity study discusses the uncertainty effects. Finally, Sec. V concludes the work and summarizes the most important findings of the paper.

II. Prerequisite Knowledge for this Study

In this section, we first elaborate on how individual emission species from aviation alter the atmospheric concentrations and what are the effects on climate change. Since not all emissions have the same effect and the effects of non-CO_2

---

[1]Air Transport Action Group (2021, November 25). Facts and Figures https://www.atag.org/facts-figures.html

[2]International Civil Aviation Organization (2021, November 25). Future of Aviation https://www.icao.int/Meetings/FutureOfAviation/Pages/default.aspx

emissions are highly dependent on the latitudes and altitudes at which they are released [10]. The second part of Sec. II focuses on the spatial and temporal dependency of non-CO_2 effects. Finally, in the same section, we introduce the improvements in aviation to date and the aircraft used in the study.

A. Aviation Emissions and Climate Change

When different species are emitted by the aircraft, they change the atmospheric concentrations/cloudiness directly or indirectly. Such changes, observed in Fig. 1, will affect the radiation balance at the top of the atmosphere indicated by the RF change. Usually, a positive RF indicates global warming and a negative RF indicates global cooling. In the following sections, the engine emissions investigated in this study are listed and described.
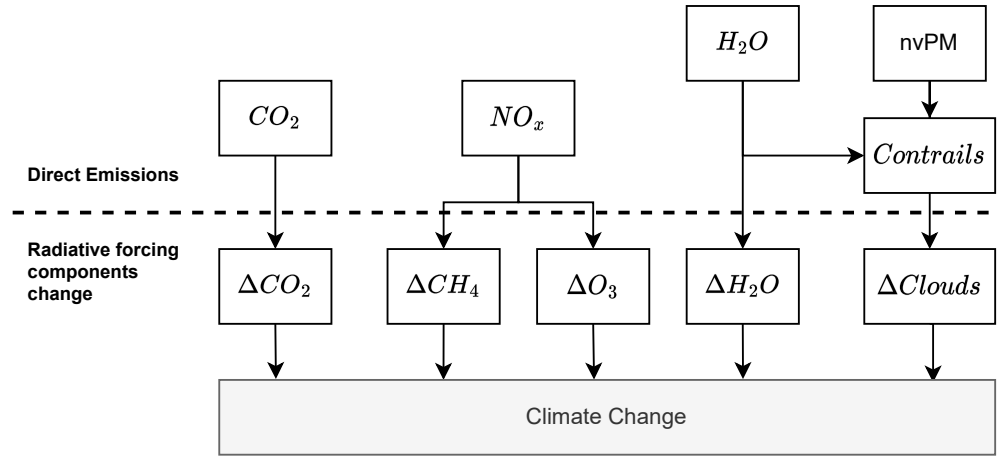

Fig. 1   Climate impact from aviation emitted species adapted from Fahey and Lee [11].

Carbon Dioxide (CO_2):

CO_2 is a product of complete combustion. Equation (1) represents the balanced chemical process for ideal combustion of hydrocarbon fuels [3]. The parameter a is the stoichiometric coefficient of the oxidizer and z is the chemical composition of air. This equation will be used later in Subsec. III.B

$$C_xH_y + a\left(O_2 + zN_2\right) \rightarrow xCO_2 + \frac{y}{2}H_2O + a \cdot zN_2 \tag{1}$$
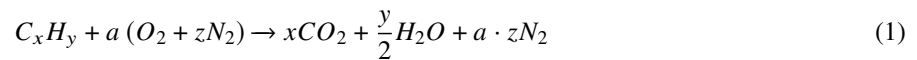
CO_2 is proportional to fuel burn and has a direct effect on climate due to the absorbance of outgoing infrared waves, increasing the temperatures in the Earth's system. The aviation CO_2 increases the atmospheric CO_2 concentration, which aggravates the warming effects from CO_2. CO_2 is one of the most emitted aviation species and its effects are long-lasting. From 1940 to 2018, CO_2 emissions alone accounted for 32% of the total RF impact from aviation species [1].

Water Vapor (H_2O):

Similar to CO_2, H_2O is a product of complete combustion and its emissions are proportional to the fuel mass burnt. Equation (1) is often used to calculate the amount of H_2O emitted per kilogram of fuel burnt, with a typical emission index of 1.25 kg/kg of kerosene.

In terms of climate impact, the total RF of H_2O is positive indicating a warming effect, but the RF of H_2O is small [12, 13]. In the case of H_2O emissions in the stratosphere, the effective RF is 2 mW/m^2 which corresponds to 2% of the total emissions. The emission of H_2O does not have a high direct consequence on the climate change, but it affects the contrail formation as shown in Eq. (2) to be discussed in following paragraph.

---

[3]The ideal combustion does not include incomplete combustion products, by-products of combustion, or products of fuel impurities, meaning that only CO_2, H_2O and N_2 are formed.

3

Non-Volatile Particulate Matters (nvPM):

Aircraft engines result in direct emissions of nvPM, which is also described as black carbon "soot" emissions [11]. Although there are many unknowns related to soot formation, there is evidence that it is related to polycyclic aromatic hydrocarbon (PAH) compounds [14, 15]. Soot formation occurs through chemical and physical processes and builds up from mostly hydrogen content to a higher carbon content [16]. Soot emissions are maximized at maximum thrust conditions [17].

nvPM from aircraft engines is regulated during the landing and takeoff (LTO) cycle due to health concerns attributed to particulate emissions. In addition to the local air quality effect, nvPM from aircraft engines can affect the cloudiness and hence the climate differently [1]. One example is that nvPM serves as nuclei for persistent contrail formation and affects the actual radiative effects of contrail [18]. In addition, the total direct soot RF was calculated to be 0.71 W/m^2 with a 90% uncertainty range [19] including all the anthropogenic soot emissions, and aviation is responsible for 0.44% of those emissions. From these numbers, the total aviation soot RF would be around 0.0031 W/m^2. This result is in line with the results from Lee et al. [20] and between the bounds dictated by Lee et al. [1].

Nitrogen Oxides (NO_x):

Although, NO_x can be a product derived from fuel impurities it is mostly treated as a by-product of combustion. NO_x is formed in the combustion chamber of the aircraft engine, and it is largely dependent on the combustion temperature, pressure, and mass flow [21]. The reduction in NO_x emissions is not as straightforward as the reduction in CO_2. Current engine design trends make efforts to increase fuel efficiency, thus decreasing CO_2 emissions. The counter effect is that, by increasing fuel efficiency[4] there is also an increase in NO_x emissions. Techniques are being investigated to reduce NO_x formation, which focus mainly on reducing combustion temperatures and combustion residence time [22]. Other methods to further reduce NO_x include multi-fuels as the primary source of energy [23, 24] and low NO_x combustion technique [25].

When discussing atmospheric chemistry and physics, it was noted that NO_x contributed to both the tropospheric O_3 production (short-term effect) and the depletion of CH_4 (long-term effect)[26]. The depletion of methane involves two long-term effects, the decrease in background ozone and the decrease in stratospheric water vapor [1]. The the short-term ozone increase, due to the emission of NO_x, yields a positive ERF of 49.3 mW/m^2. The methane decrease yields a negative ERF of -21.2 mW/m^2. The long-term ozone decrease yields a negative ERF of -10.6 mW/m^2 and the stratospheric water vapor decreases yields a negative ERF of -3.2 mW/m^2 [1]. NO_x emissions have a high climate impact; therefore, it is necessary to model them accurately. Different methods exist to calculate the amount of NO_x emitted, which depend on the amount of information known about the engine and the flight conditions [21].

Contrails:

Contrails are trails of condensed water formed behind the aircraft. There are two different types of contrails, aerodynamic and exhaust contrails. The aerodynamic contrails occur at surfaces due to a change in pressure [27]. Exhaust contrails occur when the hot and moist plume at engine exhaust mixes with the cold ambient air under favorable weather conditions (-38ºC of the ambient temperature) and will persist when supper-saturation with respect to ice is reached [28]. The contrail formation conditions can be identified using the well-know Schmidt-Appleman Criterion (SAC) as visualized in Fig. 2 [29]. The red dashed line in the figure represents isobaric mixing process of the engine exhaust and ambient, the red cross, the end of the line, represents the atmospheric conditions. The two solid lines indicate the saturation with respect to water (blue) and ice (black). Together, they define: 1) if contrails are short-lived (green area); 2) if contrails are persistent (red area). The persistent contrails can further spread into contrail cirrus [7].

The slope of the mixing line can be calculated with Eq. (2). c_P is the specific heat of air at constant pressure, P is the ambient pressure, ϵ is the ratio of the molar mass of water and air, EIH_2O is the H_2O emission index in kg/kg(fuel), Q is the fuel-specific heat and η is the overall propulsion efficiency. One can observe that the mixing process (i.e., the slope of the mixing line) depends on the aircraft/engine technology, the fuel type given the right atmospheric conditions.

$$G = \frac{c_P P}{\epsilon} \frac{EIH_2O}{Q(1-\eta)} \tag{2}$$

Furthermore, warm exhaust gases mix with the cold ambient air, resulting in liquid saturation and the nucleation of ice crystals [31]. To nucleate, the ice crystals involve aerosol particles. The number of ice crystals formed depends

---

[4]Fuel efficiency is usually increased by augmenting the combustion temperature [21].
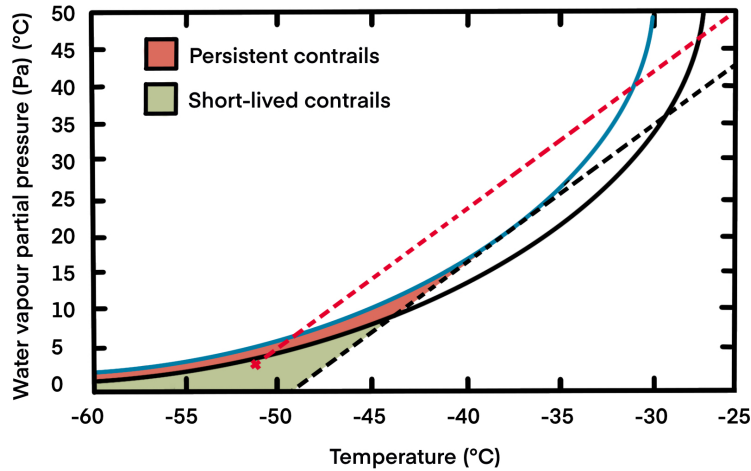
Fig. 2   Schmidt-Appleman Criterion where the *x*-axis is the temperature and the *y*-axis is the water vapor partial pressure. The black dashed line indicates the warmest temperatures for contrail formation [30].

greatly on the aerosol radius [32] and the concentration of aerosols in the jet exhaust and air [7, 33]. The aerosol particle characteristics also influence the actual RF of contrails. Global warming from contrails occurs when radiation from the Earth is scattered back to the surface. Similarly, clouds can reflect the sun's radiation to space. The ability to reflect or to absorb radiation is measured by the optical depth of the cirrus, which is defined as the degree to which it modifies the light passing through it. The optical depth of the contrails depends on the ice crystal number density, effective ice crystal radius, and ice mass content [27], therefore, the composition of the contrail cirrus is very important to understand its climate effect.

B. Climate Impact and Region of Emission
The climate impact of non-CO_2 effects, such as NO_x, H_2O and contrails, depends greatly on the time and location of the emissions [10]. Special attention should be given to the latitudes and altitudes, while the variation in terms of longitude is less dominant, highlighting the importance of investigating a wide variety of locations and altitudes around the globe.

The climate impact of H_2O depends mostly on the altitude; the higher the altitude, the higher the surface temperature change for a given amount of emission [10] due to the change in the lifetime of H_2O. At higher altitudes in the atmosphere, the residence times of H_2O are longer. NO_x emissions have a higher impact at 10-12 km altitude leading to a 200% greater ozone increase and 40% stronger methane depletion per emitted mass of NO_x than at 5 km [26, 34]. Probability of contrail formation is dependant on the altitude and latitude. The largest probability of contrail formation is found at around 9 kilometer altitude close to the poles, and at 14.5 kilometers at the equator. These areas correspond to the atmospheric areas of higher relative humidity calculated in Thatcher and Jablonowski [35]. These are the areas that should be avoided during the flight routes.

C. Hydrogen Aircraft
Hydrogen (H_2) has been proposed for commercial aviation previously in several projects due to its high specific energy density [36, 37]. Hydrogen has a Lower Heating Value (LHV) of 120 kJ/g, which is about three times higher than that of kerosene. Nevertheless, the density of hydrogen in gaseous form at 283 K is 0.08988 kg/m^3, while the density of kerosene is around 811 kg/m^3. Hydrogen can be liquefied under certain combinations of pressure and temperature to increase its density significantly (about 70.8 kg/m^{3}[5]). Still, the low density poses challenges in hydrogen storage.

---

[5]National Institute of Standards and Technology (2021, November 13) Reference Fluid Thermodynamic and Transport Properties Database (REFPROP), https://www.nist.gov/srd/refprop

1. Hydrogen Emissions

The emissions of burning hydrogen differ from the ones resulting from kerosene combustion. As commented before, for the hydrogen combustion, carbon species are not expected in the exhaust, which eliminates CO_2, CO, UHC, and Soot. The lack of aromatics in the fuel also eliminates SO_x formation. The chemical equation for ideal hydrogen combustion is represented in Eq. (3) [38].

$$H_2 + a\frac{1}{2}\left(O_2 + zN_2\right) \rightarrow H_2O + (a-1)\frac{1}{2}O_2 + a \cdot \frac{z}{2}N_2 \tag{3}$$
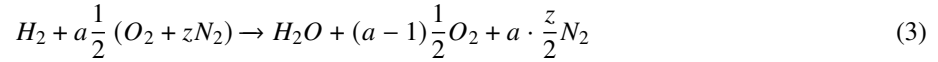
The climate drivers expected from actual hydrogen combustion are: H_2O, NO_x, and contrails. Larger quantities of H_2O and NO_x are emitted when burning a kilogram of hydrogen compared to a kilogram of kerosene. Therefore, it is crucial to investigate the climate effects of a more substantial emission index of H_2O and NO_x, and due to the higher water vapor content, revise the contrail formation probability.

H_2O emissions are increased when burning hydrogen, compared to kerosene. Gauss et al. [13] states that cryoplanes emit 2.55 times more kilograms of H_2O in flight than kerosene aircraft (hydrogen EIH_2O of 9 compared to a kerosene EIH_2O of 1.25) and its impact on climate depends on the region of emission. Increasing the cruise altitude by one km almost doubles the accumulated water vapor in the atmosphere.

NO_x emitted per kilogram of fuel ($EINO_x$) is higher for hydrogen combustion due to the higher flame temperature of hydrogen compared with kerosene. Funke et al. [8] defines a 30% increase in hydrogen $EINO_x$. Techniques to reduce it have been investigated by Carter [39], Funke et al. [8] and Sorokin et al. [40]. Lean combustion can reduce hydrogen $EINO_x$ by 24% [39] and micromix combustion by 80 to 95% [8, 40]. Due to the large discrepancies in the possible outcome of hydrogen $EINO_x$, it will be subject to a sensitivity analysis in Subsec. IV.D. Nonetheless, it is important to remember that hydrogen has almost three times more energy per kilogram of fuel, and therefore NO_x emissions will also be reduced by three. The studies observed a reduction in NO_x emissions on turbofans by burning hydrogen and kerosene from 57.94% to 68.25% [41, 42].

Contrail formation depends on atmospheric, aircraft, fuel characteristics, and the number of aerosol particles present in the exhaust. The use of cryoplanes will alter the fuel characteristics and the number of aerosol particles. As mentioned before, hydrogen has a higher EIH_2O, increasing the probability of contrail formation (according to Eq. (2)). However, hydrogen combustion does not produce aerosol particles which serve as nuclei for the ice crystals to form [13]. Recent studies from Burkhardt et al. [18], Grewe et al. [24], Boretti [43] suggest a lower contribution to global warming from hydrogen contrails due to the reduced number of soot. Some studies suggest that aerosol particles present in the air might also serve as nuclei [33]. However, the number of soot particles in the plume of an aircraft is 4 orders of magnitude larger than the concentration of black carbon particles in the atmosphere [44]. Marquart et al. [45] considered the reduction in optical depth (visibility) as another factor that altered hydrogen contrails, predicting a radiative forcing difference of ±30% compared to conventional contrails. With all these factors taken into account, Grewe et al. [24] assumed a 40% reduction on formation and radiative forcing of contrails with a reduction of 80% in soot particles. Moreover, Burkhardt et al. [18] states that, for a low soot scenario, if crystal formation is reduced by 90% a total of 69% reduction in radiative forcing can be achieved. Due to the high variability of this parameter it will be included in the sensitivity analysis in Subsec. IV.D, where the results from Marquart et al. [45] will be tested.

2. Aircraft Used in the Study

The Aerospace Technology Institute[6] is promoting transformative technology in air transport. Their project FlyZero includes a road-map aiming to realise zero-carbon emission of commercial aviation by 2030. Beddoes et al. [9] proposed different aircraft designs for the regional, narrowbody, and widebody market segments. The motivation to introduce hydrogen technology in the widebody sector is induced by the small number of major airports, which will reduce the initial hydrogen infrastructure costs and will ease the entry into service. This study will focus on the widebody, midsize hydrogen concept displayed in Fig. 3a, from here on referred to as the FZM1G aircraft. The B767-2030, displayed in Fig. 3b, is the kerosene alternative and is a future aircraft design using 2030 technology. More information about these aircraft can be found in App. V.A.

Figure 3a displays in green the hydrogen tanks, which have to be located outside the engine rotor failure zones where bird strikes might affect the airplane and general crashworthiness. The tank position was designed to allow for sufficient longitudinal stability during the flight phases. To increase tank space the fuselage diameter has been increased, which will cause slightly higher zero-lift drag compared with the kerosene aircraft.

---

[6]Aerospace Technology Institute (2022, June 06) https://www.ati.org.uk/

(a) FZM1G hydrogen aircraft.

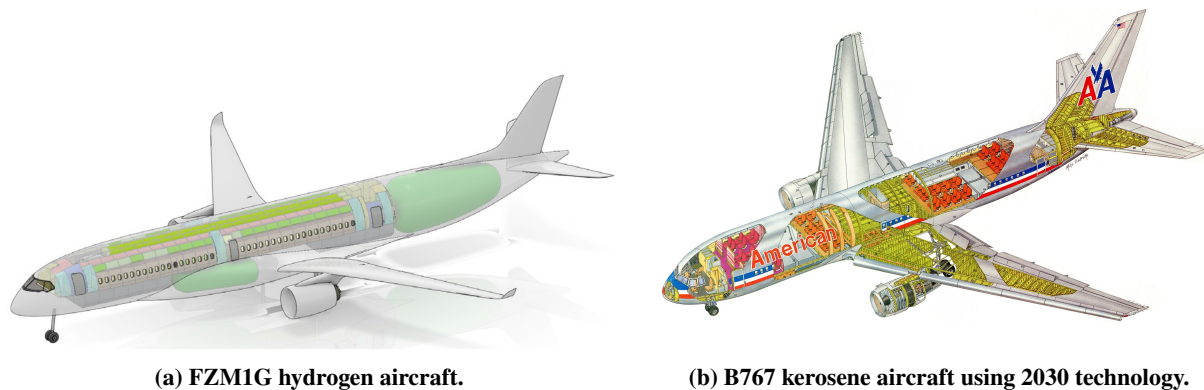(b) B767 kerosene aircraft using 2030 technology.

Fig. 3   Aircraft used in the study designed by the Aerospace Technology Institute [9].

III. Methodology

This research evaluates the impact on climate change of the FZM1G using hydrogen combustion. Figure 4 displays an overview of the research methodology of the study and how information passes through the different modules to calculate the climate change. The inputs required for the study include the aircraft to be analyzed and a flight database to create a routing network. The flight database is used because, as mentioned in Subsec. II.B, non-CO2 effects are dependent on location of emissions, and therefore, specific flight routes must be analyzed.
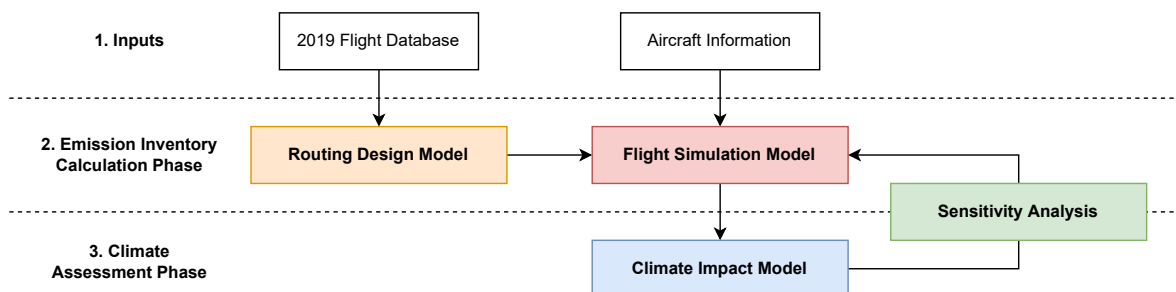

Fig. 4   Overview methodology chain for climate assessment of hydrogen aircraft composed of different modules differentiated by color.

A. Emission Inventory Calculation

The emission inventory calculation phase calculates the species emitted by the aircraft flying specific routes. The flight location is set using the routing design model and the emissions are calculated by the flight simulation model.

The **routing design model** uses the 2019 flight database from FlightRadar24[7], the data however had to be filtered, organized and converted to flight points. The relevant information of the original data included the aircraft flying the route and the origin and destination airports. Extra airport data[8][9][10] was used to place those airports in the globe and the package geographiclib[11] was used to calculate, using a great circle trajectory, the waypoints to be followed by the aircraft. Finally, to come up with a significant sample of emissions, 2.24 million flights between 1128 city pairs have been simulated. These flights are displayed in Fig. 5.

The **flight simulation model** workflow structure is presented in Fig. 6. The information used by the flight simulation model is obtained from the fleet design and the routing design. When a certain route is selected, the total range is used to compute the initial weight of the aircraft (Initial Weight Estimator). Moreover, the aircraft speed and rate of climb and

---

[7]FlightRadar24 (2021, November) Live Air Traffic https://www.flightradar24.com

[8]OurAirports (2021, November 14). Open data downloads https://ourairports.com/data/

[9]Partow, A. (2021, November 14) The Global Airport Database https://www.partow.net/miscellaneous/airportdatabase/

[10]OpenFlights.org (2021, November 14) Airport, airline and route data https://openflights.org/data.html

[11]Karney, C. (2021, November 23). Geographiclib 2.0 Documentation https://geographiclib.sourceforge.io/html/python/
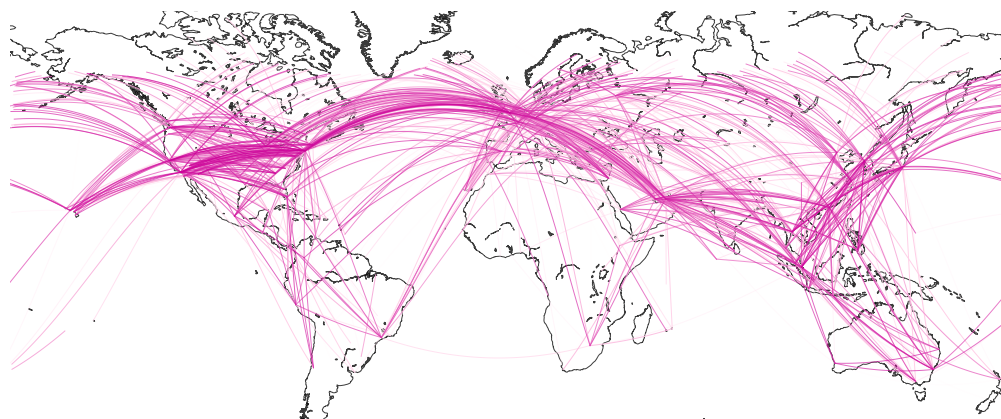
Fig. 5   Flight map with 1128 city pairs and 2.24 million flights, the frequency of the flights is represented by the line colour intensity.

descent are used to compute the flight plan (Flight Planner). When the flight iteration begins, the state of the aircraft is ran through a module which declares what the aircraft should do next (Auto Pilot). The three possible states are, climb, cruise or descent. Then the state of the aircraft is ran through the flight dynamics model which calculates the aircraft speed, altitude, time step, flight path angle, drag and thrust using the energy equations from Eurocontrol [46]. An engine deck is used to rapidly convert the engine thrust in fuel flow, temperature and pressure before the combustion chamber. Two engine decks were computed using the engine model from Proesmans and Vos [47], one for kerosene and one for hydrogen. The values on the engine deck are used to compute the NO_x emission index ($EINO_x$) emitted at every step of the flight and to update the fuel weight of the aircraft. Next, the aircraft weight and the flown distance are updated. When the flown distance equals the total range of the flight, the extra fuel weight is computed (contingency fuel). If the fuel remaining is $\pm$ 10 % of the required contingency fuel (5% of the consumed fuel), the simulation is finished, and the next route can be analyzed. More information on the method used to compute NO_x emissions can be found in App. V.B.

When all the flights have been simulated, an emission inventory with the following information is created: longitude and latitude in degrees, pressure altitude in hectopascals, fuel burn and NO_x emitted in kilograms, flown distance in kilometers and time frequency in times flown per year. This will serve as input in the climate impact model. The resulting distribution of flights in latitudes and altitudes can be observed in Fig. 7a and Fig. 7b respectively. There is considerably more flights in the temperate zones (between the North Pole and the Tropics) than in any other latitude of the world. This area corresponds to the latitudes at which Europe, the United States and China are located. Figure 7b displays the flight occurrences at different altitudes for the B767S aircraft. It can be observed that most of the flight points occur close at the cruise altitude (264 hPa). It is important to mention that the two aircraft fly at slightly different altitudes, the FZM1G flies at 10.7 km while the B767S at 10 km. More information about the fleet design parameters can be found in App. V.A. The rest of the flight points represent the aircraft climbing and descending, also included in the study.

B. Climate Assessment

The climate assessment phase calculates the temperature response with the emission inventory. This subsection describes the tool selected to perform this calculation, states the changes in methodology to adapt the module for hydrogen use, and explains the scenario selected which will will set the bases for a fair comparison between the aircraft of the study.

1. Climate Assessment Tool

Several tools were investigated to convert the previously generated emission inventory into climate change metrics, namely: Climate and Aviation Sustainable Trajectories (CAST) developed by Planès et al. [48]; Model for the Assessment of Greenhouse Gas Induced Climate Change (MAGICC) developed by Meinshausen et al. [49]; LinClim developed by Lim and Lee [50]; and AirClim developed by Grewe and Stenke [10]. The potential models were listed by ICAO[12]. The

---

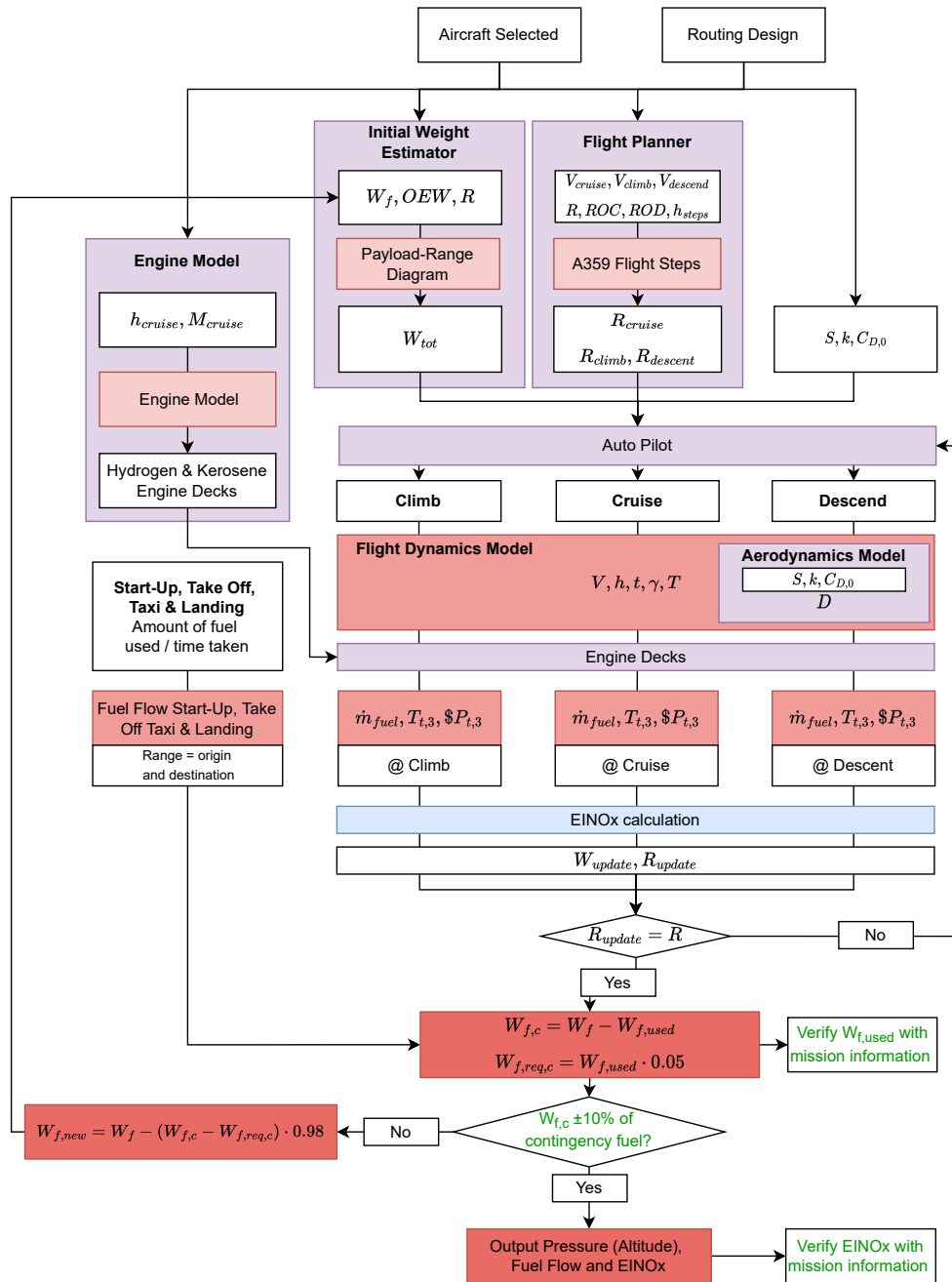[12]International Civil Aviation Organization (2021, November 24). Models and Databases https://www.icao.int/environmental-protection/pages/modelling-and-databases.aspx

Aircraft Selected

Routing Design

Initial Weight Estimator

W_f, OEW, R

Payload-Range Diagram

W_{tot}

Flight Planner

$V_{cruise}, V_{climb}, V_{descend}$
R, ROC, ROD, h_{steps}

A359 Flight Steps

R_{cruise}
$R_{climb}, R_{descent}$

$S, k, C_{D,0}$

Engine Model

h_{cruise}, M_{cruise}

Engine Model

Hydrogen & Kerosene Engine Decks

Start-Up, Take Off, Taxi & Landing
Amount of fuel used / time taken

Fuel Flow Start-Up, Take Off Taxi & Landing

Range = origin and destination

Auto Pilot

Climb

Cruise

Descend

Flight Dynamics Model

V, h, t, γ, T

Aerodynamics Model

$S, k, C_{D,0}$

D

Engine Decks

$\dot{m}_{fuel}, T_{t,3}, \$P_{t,3}$

@ Climb

$\dot{m}_{fuel}, T_{t,3}, \$P_{t,3}$

@ Cruise

$\dot{m}_{fuel}, T_{t,3}, \$P_{t,3}$

@ Descent

EINOx calculation

W_{update}, R_{update}

$R_{update} = R$

No

Yes

$W_{f,c} = W_f - W_{f,used}$
$W_{f,req,c} = W_{f,used} \cdot 0.05$

Verify $W_{f,used}$ with mission information

$W_{f,new} = W_f - (W_{f,c} - W_{f,req,c}) \cdot 0.98$

No

$W_{f,c} \pm 10\%$ of contingency fuel?

Yes

Output Pressure (Altitude), Fuel Flow and EINOx

Verify EINOx with mission information

Fig. 6   Flight simulation methodology for climate assessment of hydrogen and kerosene aircraft.

9

(a) Latitude distribution of flight data points with marks on temperate zones, the Tropics and frigid areas.

(b) Altitude distribution of flight waypoints given in hectopascals.
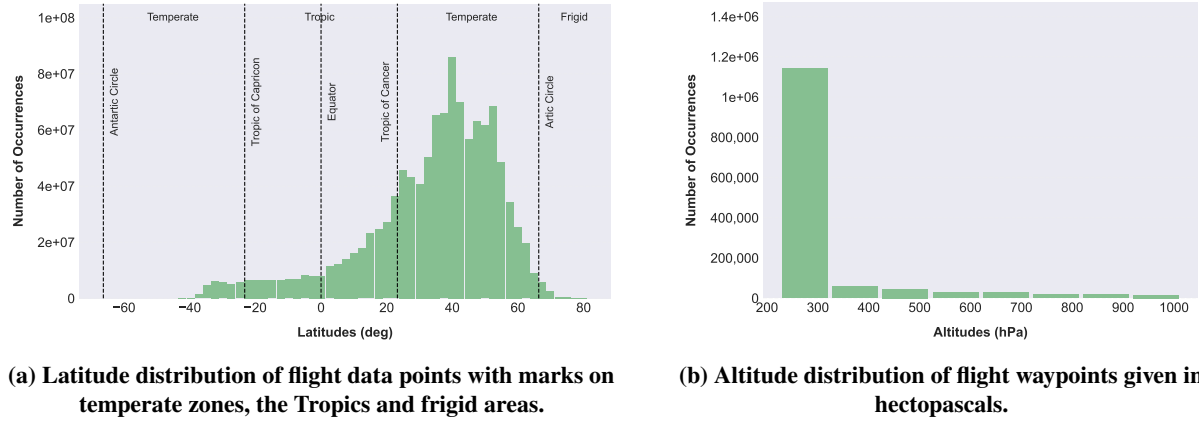
Fig. 7   Latitude and altitude flight point distribution for the B767S.

selection narrowed down to availability, versatility, and relevance of the output climate metric. With these three factors in mind AirClim was selected.
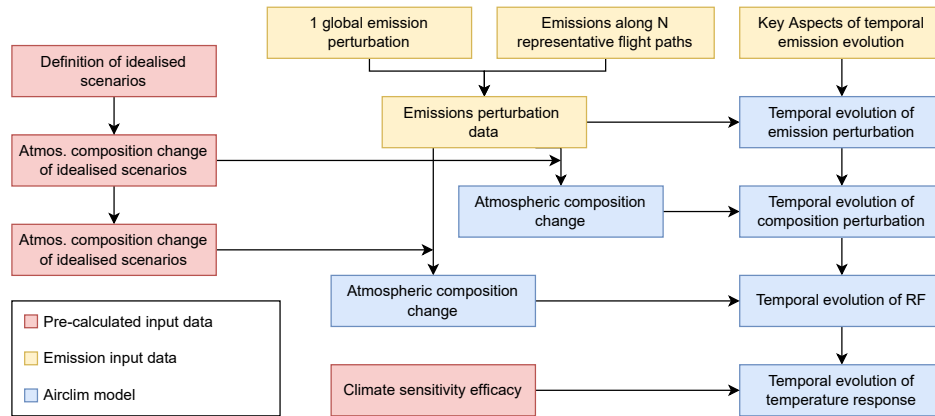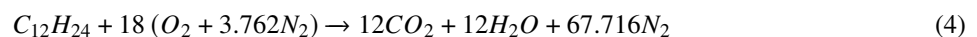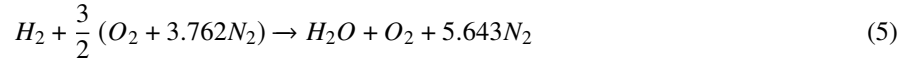

Fig. 8   AirClim model architecture with dependencies between the three different modules [10].

AirClim evaluates the climate impact of CO_2, NO_x, H_2O and contrails. AirClim is divided into three different modules, as shown in Fig. 8. The main model is displayed in blue, for which the input is the precalculated chemistry input data in red and the emission from the aircraft trajectory in yellow. The precalculated input data module (red) consists of three steps: the first one defines the emission regions with a normalized emission strength; the second step performs a climate chemistry simulation with the chemistry model E39/C; finally, the third step calculates the radiative forcing of each perturbation scenario. The perturbation scenarios are calculated from the emission input data (yellow). AirClim allows for an emission inventory with distributed emissions along a 3D path (a flight route). The linear response model AirClim (blue) combines the precalculated input data (red) with the emission data (yellow) to calculate the changes in near-surface temperature. The AirClim model also uses a background aircraft scenario to isolate the change in temperature from the new technology. A more insightful explanation of the model is presented in Grewe and Stenke [10] and Dahlmann et al. [6]. The final output from AirClim is a temporal evolution of the near-surface temperature change.

AirClim assumes that the fuel specified in the emission inventory is kerosene and thus the tool has to be adapted to analyse hydrogen. As explained in Sec. II, the emissions of hydrogen combustion are different than those of kerosene. AirClim states EI for these which can be modified to work with hydrogen. Equation (4) and Eq. (5) represent the chemical balanced equations for kerosene and hydrogen combustion respectively and have been obtained from Eq. (1) and Eq. (3). Using the molar masses of each element the emission index of each of the species can be calculated.

$$C_{12}H_{24} + 18\,(O_2 + 3.762N_2) \rightarrow 12CO_2 + 12H_2O + 67.716N_2 \tag{4}$$

$$H_2 + \frac{3}{2}(O_2 + 3.762N_2) \rightarrow H_2O + O_2 + 5.643N_2 \qquad (5)$$

The $EICO_2$ for kerosene is 3.155 kg per kg of fuel and for hydrogen is 0. The EIH_2O for kerosene is 1.29 kg per kg of fuel and for hydrogen is 9 kg/kg. Table 1 also includes the contrail RF change as defined in Sec. II due to soot reduction.

Table 1   Hydrogen and kerosene species modifications for AirClim.

Fuel	Contrail RF Change	$EICO_2$	EIH_2O
Kerosene	-	3.155	1.25
Hydrogen	- 69%	0	9

2. Future Traffic Scenario

As suggested by Grewe et al. [24] it is important to understand the climate objective before setting an scenario. The study is set to compare purely the technology, that is why in Table 2 the simulation start year coincides with the FZM1G and B767S introduction year. Moreover, to make it comparable to other studies, the simulation end year was set to 2130. Aviation market growth is understood as the change in Revenue Passenger Kilometer (RPK), assumed to grow by 6.0% from 2019 to 2025 according to ICAO, by 1% from 2050 to 2075 and by 0.8% from 2075 to 2130 when the simulation stops [51] to maintain business as usual (BAU). It is important to note that we are not only interested on the growth for this analysis but more importantly on the fuel consumption, for that, fuel efficiency improvements over the years are included. Finally, in this study it is assumed that the aircraft entrance in the market is instantaneous, which will ease the calculation of the results and the direct comparison of the kerosene and hydrogen aircraft. Please note that, the aviation growth is assumed from 2019 because is the year for which the flight data was available.

Table 2   Scenario assumptions used for the comparison of the climate change caused by the hydrogen and kerosene aircraft.

Scenario Parameters	Value	Scenario Parameters	Value
Simulation Start Year	2030	Simulation End Year	2130
B767S (ker) Start Year	2030	FMZ1G (hyd) Start Year	2030
Market Growth BAU (2019-2025)	6.0%	Market Growth BAU (2025-2050)	1.2%
Market Growth BAU (2050-2075)	1.0%	Market Growth BAU (2075-2130)	0.8%

IV. Results

Table 3 displays the emissions caused by the hydrogen and kerosene aircraft relative to energy, flown distance and passengers displaced. We can observe that the kerosene aircraft (B767S) is consuming 2.5 times more fuel than the hydrogen aircraft (FZM1G) in terms of mass. This difference is mainly caused by the difference between the hydrogen and kerosene energy density, being 2.79 times larger for the hydrogen fuel. This disparity can be observed in the energy used per km column, where the hydrogen aircraft requires 12% more energy to travel the same distance. This is caused by three reasons, the engine specific energy consumption, being slightly larger for the hydrogen aircraft (593 $J/s/N$ vs 581 $J/s/N$), the larger OEW of the hydrogen aircraft, making the average thrust on the typical mission flight higher (70 kN vs 64 kN), and the larger wetted area of the hydrogen aircraft required to fit the large tank volume. Figure 9 represents the influence on climate warming of the kerosene and hydrogen aircraft. The ever increasing temperature is due the selected BAU scenario, where there is a continuous increase in demand and therefore in flights and fuel consumed.

The surface temperature increase after 100 years caused by the kerosene-fueled aircraft (B767S) is 18.9 mK, while for the hydrogen combustion aircraft (FMZ1G) is 6.3 mK (67% lower). Figure 9 draws the Paris Agreement goals represented by the dashed black line at 2.4 mK, calculated with the proportional share of the selected flights with respect to the total CO_2 emissions. It can be observed that both aircraft fail to keep the temperature increase below this number, however, whereas the B767S surpasses the 2.4 mK temperature increase only 3 years after its implementation,

Table 3   Fuel used by the FZM1G and the B767S on all routes.

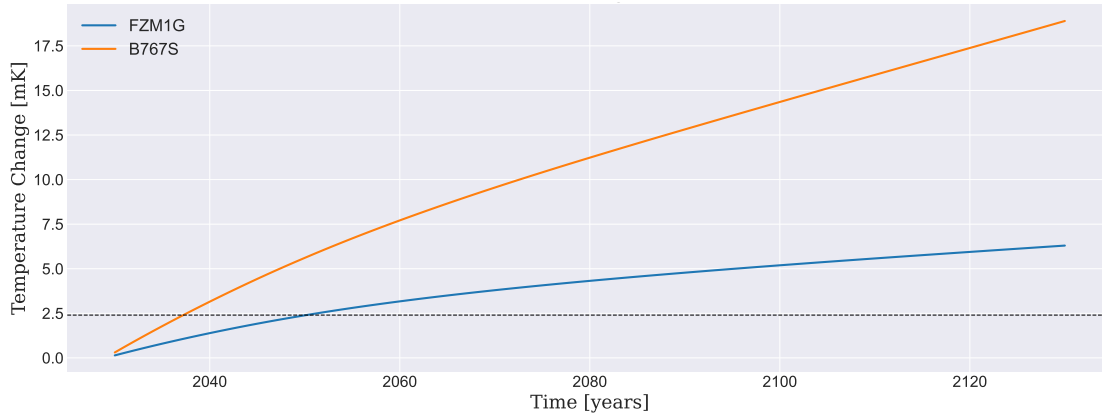| Aircraft Type	Fuel Burnt	Fuel Burnt per km	Energy Used per km	Fuel Burnt per km per Pax.
Unit	Mt	kg/km	MJ/km	kg/km/pax
FZM1G	16.7	1.45	174	0.0052
B767S	41.5	3.62	156	0.0130

Fig. 9   Change in surface temperature caused by the FMZ1G and B767S. The dashed line corresponds to the maximum temperature increase the fleet should cause to meet the climate objectives stated in the Paris Agreement.

the hydrogen aircraft FMZ1G surpasses the line 20 years later. In Fig. 9 the development of the temperature change over the years can be observed, however this will be treated further in the results, knowing more information on the climate effect from individual species. The next sections will provide an in-depth assessment on the reasons why such a deviation is observed.

A. Climate Effect from Individual Emission Species

It is important to know the differences in emitted species between the B767S and the FMZ1G, as Table 3 only gives information about the fuel consumed. Table 4 displays the different emissions and emission indexes per aircraft. It can be observed that the emission index is now represented first as the emitted species per kilogram of fuel and secondly as the emitted species per energy consumed.

Table 4   Species emitted and fuel consumed by the FZM1G and B767S.

Aircraft	Fuel	NO_x	$EINO_x$		CO_2	$EICO_2$		H_2O	EIH_2O	
	Mt	kt	g/kg	g/MJ	Mt	kg/kg	kg/MJ	Mt	kg/kg	kg/MJ
FZM1G	16.7	179	10.8	0.0898	0	0	0	150	9	0.075
B767S	41.5	544	13.1	0.305	131	3.155	0.734	51.8	1.25	0.029

NO_x emissions from kerosene are three times higher than emissions from hydrogen. However, it must be noted that NO_x was calculated based on fuel burnt, and thus 82% of the difference comes from the larger quantity of kerosene burnt compared with hydrogen. $EINO_x$ should reduce by 25% in hydrogen combustion by taking advantage of the lower lean limit of hydrogen, however, it is only reduced by 18% due to the effects of Mach and altitude as discussed in App. V.B.

Figure 10 displays how different species contribute to climate change by 2130. The sudden increase in temperature change in Fig. 9 for both aircraft occurs due to the sudden introduction of the fleet in the market as explained in the future traffic scenario definition. As can be observed, effects of hydrogen aviation on temperature rise are lower than
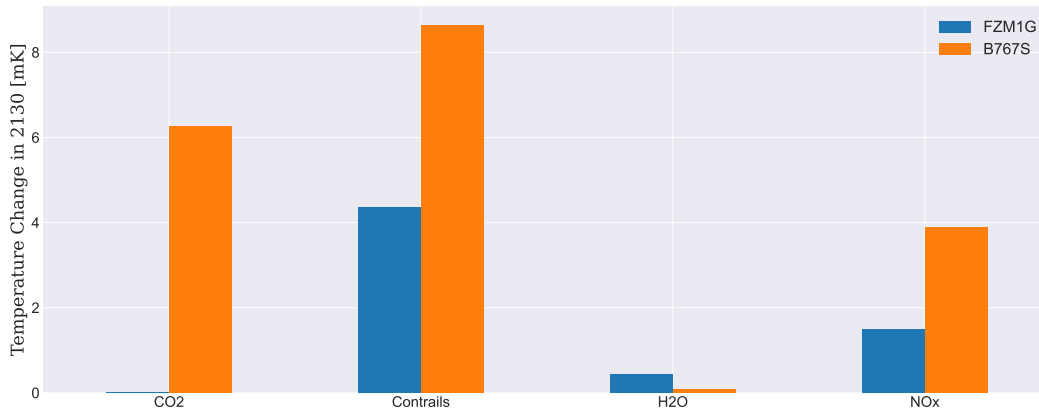
12

Fig. 10   Contribution to surface temperature increase from each of the species per aircraft model.

those of kerosene aviation, with several considerations. Contrail effects are the largest individual contributor to surface temperature change for both kerosene and hydrogen aircraft. The temperature change due to contrails is considerably smaller for the hydrogen aircraft (50% lower). This reduction is caused mainly by the 69% reduction in radiative forcing due to soot elimination for hydrogen combustion, and due to the reduction in overall efficiency of the hydrogen aircraft (0.40 vs 0.41, affecting the contrail formation probability). On the other hand, the higher cruise altitude causes an increase in surface temperature change due to the formation of contrails. Moreover, the higher water vapour content on the hydrogen engine plume increases the contrail formation probability. CO_2 effects are only present for the kerosene aircraft (B767S), these effects will be better reflected when talking about the temporal evolution in Subsec. IV.B. H_2O climate effect is 4.7 times higher for the hydrogen aircraft, which has to do with the higher emission index of hydrogen combustion as seen in Table 4, but also with the higher altitude of the hydrogen aircraft, causing a larger temperature increase. Temperature increase from NO_x emissions is 2.6 times larger for kerosene aircraft. We can observe that the emissions of NO_x are 67% lower, however, the climate impact is only 61% lower. The difference is caused by the altitude, increasing the change in surface temperature the higher in the atmosphere NO_x is emitted (where the hydrogen aircraft is flying), as will be discussed in subsection IV.D.

B. Trend Over Time of Temperature Response for Individual Species

Emissions can be differentiated on how fast they have an effect on climate and how long do they remain in the Earth's system. CO_2 is a long-lived species, therefore it has an effect on climate years after of being emitted. Moreover, CO_2 effects on climate are not instantaneous, and some years might be required for the surface temperature change to start increasing (as shown in Fig. 11). Contrails on the other hand have a shorter life. In Fig. 12 it can be observed that the delta temperature increase of contrails is reduced with time, following the aviation market. This occurs because contrails dissipate in hours or days after the formation (short-lived).
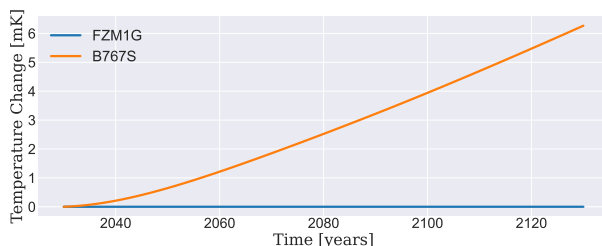

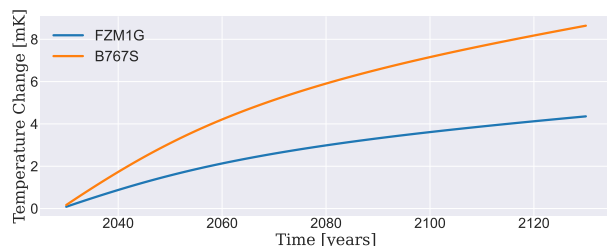**Fig. 11   Surface temperature increase caused by CO_2 for the B767S and FZM1G.**

Fig. 12   Surface temperature increase caused by contrails for the B767S and FZM1G.

NO_x effects are slightly more complicated; when released in the atmosphere, NO_x causes both a production in ozone and a depletion of methane (causing consequently both an increase and a reduction in temperature). These compounds

are very reactive, which causes a faster interaction with climate change at the beginning of the simulation than any other species (Figure 13). It can also be observed that NO_x follows a similar trend to that of contrails due to its short life. H_2O effects on temperature are similar to the contrail effects, with a fast reaction at the beginning and a non-cumulative behaviour.
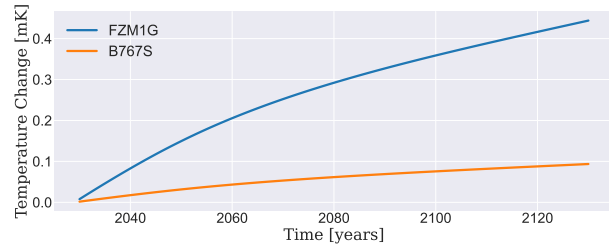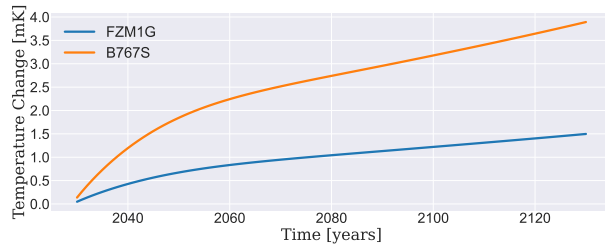

Fig. 13   Surface temperature increase caused by NO_x emissions for the B767S and FZM1G.

Fig. 14   Surface temperature increase caused by water vapour emissions for the B767S and FZM1G.

These results lead to an important conclusion, hydrogen does not emit the species causing the largest cumulative behaviour (CO_2), this means that, if for any reason the hydrogen fleet is stopped, the surface temperature recovery is expected to be faster for a hydrogen aircraft. Figure 15 demonstrates these effects.
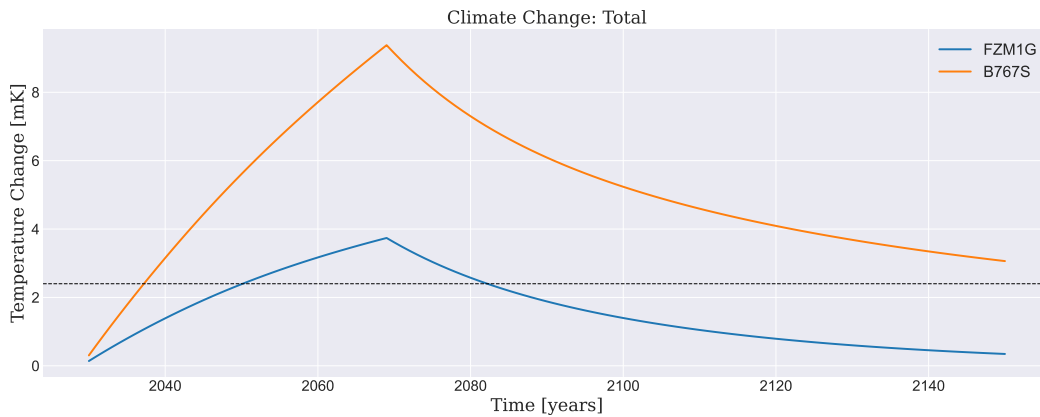

Fig. 15   Temperature increase caused by the B767S and FZM1G and climate recovery when flights are stopped after 2070.

Until 2070, the same trend as in Fig. 9 is observed. The trend differs once flights are stopped. Initially, the surface temperature change caused by the B767S reduces considerably. At the end of the simulation, temperature has been increased by 3.1 mK (CO_2 causes 2.4 mK and the rest is caused mostly by NO_x). FZM1G shows a slower initial surface temperature decay due to the lower climate effect of contrails, water vapour and NO_x. However, at the end of the simulation, temperature has been increased only by 0.34 mK due to the lack of CO_2 climate effects.

C. Regional Effects of Non-CO2 Emissions

All emission climate effects except for CO_2 depend greatly on the latitude at which the species are emitted. To investigate these effects, flight points were divided into three different zones, frigid latitudes greater than 66.34º North/South, temperate latitudes between 66.34º and 23.26º North/South, and tropical latitudes lower than 23.26º North/South. CO_2 climate effects are not dependent on geographical location, as such, they will be excluded from the analysis in this section.

Table 5 displays the total surface temperature change for the different latitudes and aircraft. The emitted species by the B767S flying over the frigid latitudes cause a 1.6% of the total temperature increase, however, for the FZM1G this percentage is 1.3%. The emitted species of the kerosene B767S flying over the tropical latitudes cause a 12.7% of the total temperature increase, however, for the FZM1G this percentage is increased to 14.0% due to the contrail effects. At

tropical latitudes, hydrogen influence on climate is relatively more detrimental[13] than kerosene alternatives, however, at frigid latitudes, the opposite is observed.

Table 5   Surface Temperature Change (STC) caused by the B767S and FZM1G at different latitudes.

	Frigid		Temperate		Tropics	
Parameter	STC	%	STC	%	STC	%
Unit	mK	-	mK	-	mK	-
B767S	0.31	1.6	16	86	2.4	13
FZM1G	0.082	1.3	5.3	85	0.88	14

Flying over the Tropics at low altitudes influences greatly the impact of the emissions on climate change, however, over frigid latitudes this altitude difference is less relevant. Nevertheless, it must be noted that these results are strongly dependent on the selected aircraft. In this case the kerosene aircraft flies at 10 km, but, if it were to fly slightly higher, differences with hydrogen aviation would be negligible due to the increase in contrail formation probability.

D. Sensitivity Analysis

A sensitivity analysis is performed to understand the effects of uncertainties on the final results. The major flight performance uncertainty is the cruise altitude, strongly linked to climate effects. Furthermore, some parameters with high uncertainty related to hydrogen emissions and climate effects were mentioned in Subsec. III.B. The sensitivity study is divided into the flight performance assessment and the hydrogen impact assessment.

E. Flight Performance Assessment

During the flight simulation, the cruise speed and cruise altitude define the flight time and the fuel consumed during the mission. The flight altitude has a clear relation to climate impact, and therefore the final results change when altering it. Altitude and speed should not be separated, as they are dependent of each other. If an aircraft is flown at a higher cruise altitude, the cruise speed should be adapted to fly at the fuel-optimum lift coefficient. Speeds with a Mach number above 0.9 are removed from the study because the drag model is unable to capture the transonic drag rise. Cruise altitudes above 11 km for this particular tube-and-wing aircraft designs require cruise Mach numbers above 0.9 at the top of climb. Table 6 displays the situations with the variable altitude and the resulting fuel consumed and Table 7 the surface temperature variation.

Table 6   Influence on fuel consumption caused by the sensitivity analysis flight performance situations.

Flight Performance Situations	Fuel Consumed [Mt]			
	FZM1G	Diff.	B767S	Diff.
Cruise Altitude 9 km	17.1	1.8%	42.8	3.1%
Cruise Altitude 10 km	16.8	-	41.5	-
Cruise Altitude 11 km	16.6	-1.2%	40.5	-2.4%

Table 7   Influence on fuel consumption caused by the sensitivity analysis hydrogen impact situations.

Flight Performance Situations	Temperature Increase [mK]			
	FZM1G	Diff.	B767S	Diff.
Cruise Altitude 9 km	3.58	-28.7%	14.7	-22.2%
Cruise Altitude 10 km	5.02	-	18.9	-
Cruise Altitude 11 km	7.34	46.2%	22.4	18.5%

---

[13]Relatively detrimental because, even though the temperature increase caused by the FZM1G is lower than the kerosene alternatives (0.883 mK vs. 2.41 mK), the sensitivity to tropical latitudes is higher.

The relation between altitude, fuel consumed and change in surface temperature is interesting. To achieve the same lift at a higher altitude, the aircraft must fly faster. This higher speed improves the engine performance, decreasing fuel consumption [52, 53]. However, the higher in the atmosphere the fuel is consumed, the larger climate effects from the emitted species. Please note that there is physical limits for the maximum altitude at which you can fly depending on cruise Mach and wing loading.

In Table 6 and Table 7 it can be observed that fuel consumption and surface temperature change are always higher for the kerosene aircraft. But it is also important to understand the implications of altitude deviations in both fuel consumption and surface temperature change. Observing the percentages on both tables, it can be noted that the hydrogen aircraft fuel consumption is less susceptible to changes on altitude. On the contrary, it's surface temperature response is more susceptible to changes on altitude. However, kerosene aircraft also includes CO_2 emissions, which do not depend on altitude and reduce the surface temperature change difference.

1. Hydrogen Impact Assessment

The sensitivity analysis can also be performed with respect to hydrogen uncertainties. The $EINO_x$ hydrogen ratio is subject to large uncertainties. The baseline situation uses a ratio between NOx emissions from hydrogen combustion to NOx emission from kerosene combustion of 0.76. This parameter represents the $EINO_x$ change due to hydrogen combustion by taking advantage of the lower lean limit of hydrogen. However, Funke et al. [8] states that it can be as low as 0.1 and as high as 1.3. The contrail radiative forcing for hydrogen combustion also has a large variability. It would be interesting to analyze deviations in this parameter to observe if the final conclusion of the study still holds. Table 8 displays the variation in NO_x emissions when varying the $EINO_x$ ratio. NO_x reduces by 87% when $EINO_x$ ratio is set to 0.1, and increases by 72% when $EINO_x$ ratio is set to 1.3.

Table 8 NO_x emitted by the FZM1G for the different situations analyzed in the sensitivity analysis.

Flight Performance Situations	NO_x Emissions [kt]
Baseline (0.75 NO_x rat.)	179
0.1 NO_x ratio	23.7
1.3 NO_x ratio	308

Table 9 displays the surface temperature increase in percentage for the situations described above. If this study has overestimated the capacity of hydrogen to reduce NO_x emissions and $EINO_x$ [14] is 1.3 times higher than for kerosene aviation, the surface temperature increases by 18%. If, on the other hand, this study has underestimated the hydrogen creation of NO_x and the ratio is 0.1 lower, the surface temperature would decrease by 20%. The contrail RF ratio is the relation between the radiative forcing of hydrogen contrails versus kerosene contrails. For the baseline case is set to 0.31, which corresponds to a reduction of 69% in the RF of hydrogen contrails compared to kerosene contrails [18]. If this ratio were to be 0.7 or even 1.3, the surface temperature change would increase. If the contrail radiative forcing ratio is increased to 0.7, the surface temperature change increases by 88% for the FZM1G. When the contrail radiative forcing is increased to 1.3, the surface temperature change increases by 220% for the FZM1G.

Table 9 Situations for the hydrogen sensitivity analysis influence on surface temperature change.

Flight Performance Situations	Temperature Increase [mK]
Baseline ($EINO_x$ ratio: 0.75, Contrail RF: 0.31)	6.34
$EINO_x$ ratio 1.3	7.37
$EINO_x$ ratio 0.1	5.00
Contrail Radiative Forcing Ratio 0.7	11.8
Contrail Radiative Forcing Ratio 1.3	20.2

For this study, it would also be interesting to know what could happen in the worst case scenario (WCS) and best case scenario (BCS) for hydrogen combustion, and compare that to the results in Fig. 9. Figure 16 includes the best

---

[14]Note that $EINO_x$ increases with resepect to kerosene aviation, however NO_x is still lower due to the reduced fuel consumption.

(FZM1G - BCS) and worst (FZM1G - WCS) estimate for the hydrogen tube-and-wing aircraft. The WCS includes the EINO$_x$ ratio of 1.3 and the contrail radiative forcing ratio of 1.3. The BCS includes the EINO$_x$ ratio of 0.1 and a contrail radiative forcing ratio of 0.31.
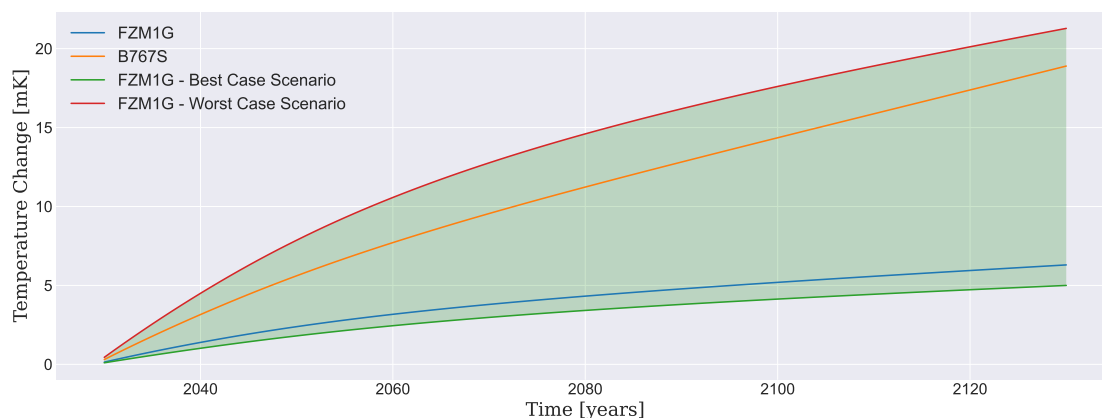

Fig. 16   Temperature change distribution for the B767S and FZM1G, including a best and worst case scenario (BCS, WCS) for the hydrogen aircraft.

At the beginning of the simulation, the worst case scenario for the hydrogen aircraft causes a higher surface temperature change with respect to the kerosene aircraft. The temperature difference increases until 2090, after that, it is reduced due to the cumulative nature of CO$_2$ emissions, as explained in Subsec. IV.B.

V. Conclusions

This study has developed a new methodology to model emissions and calculate the surface temperature change caused by a long-range, twin-aisle, tube-and-wing aircraft fleet using hydrogen and kerosene combustion. The chosen aircraft were flown over relevant flight routes, selected using the routing design model, based on global coverage and aircraft mission specifications. An emission inventory, composed of consumed fuel and nitrogen oxide emissions per flight step, was calculated using a flight simulation model. Using a climate impact model, the surface temperature change for both the hydrogen and kerosene aircraft was obtained. Results show that the hydrogen fleet would consume 16.7 megatons of hydrogen for the 2.2 million flights simulated, while the kerosene fleet would consume 41.5 megatons. However, the hydrogen aircraft consumes 12% more energy per seat per kilometer, mainly due to its higher wetted area resulting from the tank integration. After 100 years of simulation, the hydrogen aircraft fleet causes a 67% lower surface temperature change than its kerosene kerosene counterpart, i.e. 6.3 mK opposed to 18.9 mK. This improvement is achieved due to the absence of carbon emissions, the lower radiative forcing of hydrogen contrails, and the reduction in NO$_x$ emissions due to the lower lean limit of hydrogen fuel. In addition, it is shown that in the hypothetical situation where flights are halted, climate recovery occurs faster for hydrogen-powered aircraft. It is also shown that hydrogen aircraft have a lower surface temperature susceptibility when flying over the poles and higher susceptibility when flying over the tropics. A sensitivity study showed that, although the fuel consumption decreases slightly at higher altitudes, the surface temperature change increases. The sensitivity of surface temperature increase to altitude was found to be higher for hydrogen aircraft than for kerosene aircraft. When the uncertainties related to hydrogen emissions and contrails were investigated, the worst case assumption induced a surface temperature change due to hydrogen aircraft that was higher than that of kerosene aircraft, with a possible reversal on the long run due to CO$_2$ elimination.

Although aviation on its own will not solve the current environmental problems, I believe hydrogen combustion has the potential to become a new milestone in the development of a much more sustainable aviation. We have observed that even the worst case situation for hydrogen aircraft is advantageous compared to kerosene aviation in the long run.

Acknowledgments

17

References

[1] Lee, D. S., Fahey, D. W., Skowron, A., Allen, M. R., Burkhardt, U., Chen, Q., Doherty, S. J., Freeman, S., Forster, P. M., Fuglestvedt, J., Gettelman, A., De León, R. R., Lim, L. L., Lund, M. T., Millar, R. J., Owen, B., Penner, J. E., Pitari, G., Prather, M. J., Sausen, R., and Wilcox, L. J., "The contribution of global aviation to anthropogenic climate forcing for 2000 to 2018," *Atmospheric Environment*, Vol. 244, No. July, 2021. https://doi.org/10.1016/j.atmosenv.2020.117834.

[2] Grewe, V., Dahlmann, K., Flink, J., Frömming, C., Ghosh, R., Gierens, K., Heller, R., Hendricks, J., Jöckel, P., Kaufmann, S., Kölker, K., Linke, F., Luchkova, T., Lührs, B., van Manen, J., Matthes, S., Minikin, A., Niklaß, M., Plohr, M., Righi, M., Rosanka, S., Schmitt, A., Schumann, U., Terekhov, I., Unterstrasser, S., Vázquez-Navarro, M., Voigt, C., Wicke, K., Yamashita, H., Zahn, A., and Ziereis, H., "Mitigating the climate impact from aviation: Achievements and results of the DLR WeCare project," *Aerospace*, Vol. 4, No. 3, 2017. https://doi.org/10.3390/aerospace4030034.

[3] Zheng, X. S., and Rutherford, D., "Fuel burn of new commercial jet aircraft: 1960 to 2019," Tech. Rep. September, The International Council on Clean Transportation, 2020.

[4] Delbeke, J., Runge-Metzger, A., Slingenberg, Y., and Werksman, J., "The Paris Agreement," *Towards a Climate-Neutral Europe: Curbing the Trend*, 2019, pp. 24–45. https://doi.org/10.4324/9789276082569-2.

[5] Clean Sky 2 and Fuel Cells and Hydrogen 2 Joint Undertaking, *Hydrogen-powered aviation - A fact-based study of hydrogen technology, economics, and climate impact by 2050*, May, Publications Office, 2020. https://doi.org/10.2843/766989.

[6] Dahlmann, K., Grewe, V., Frömming, C., and Burkhardt, U., "Can we reliably assess climate mitigation options for air traffic scenarios despite large uncertainties in atmospheric processes?" *Transportation Research Part D: Transport and Environment*, Vol. 46, No. 2, 2016, pp. 40–55. https://doi.org/10.1016/j.trd.2016.03.006, URL http://dx.doi.org/10.1016/j.trd.2016.03.006.

[7] Kärcher, B., "Formation and radiative forcing of contrail cirrus," *Nature Communications*, Vol. 9, No. 1, 2018, pp. 1–17. https://doi.org/10.1038/s41467-018-04068-0, URL http://dx.doi.org/10.1038/s41467-018-04068-0.

[8] Funke, H., Beckmann, N., and Abanteriba, S., "An overview on dry low NO x micromix combustor development for hydrogen-rich gas turbine applications," *International Journal of Hydrogen Energy*, Vol. 44, 2019, pp. 6978–6990. https://doi.org/10.1016/j.ijhydene.2019.01.161.

[9] Beddoes, S., Foster, M., James, D., Kay, E., Kay, O., Shawki, K., Stubbs, E., Thomas, D., Weider, K., and Wilson, R., "FlyZero-Zero-Carbon Emission Aircraft Concepts," Tech. rep., Aerospace Technology Institute, 2022. URL https://www.ati.org.uk/flyzero-reports/.

[10] Grewe, V., and Stenke, A., "AirClim: An efficient tool for climate evaluation of aircraft technology," *Atmospheric Chemistry and Physics*, Vol. 8, No. 16, 2008, pp. 4621–4639. https://doi.org/10.5194/acp-8-4621-2008.

[11] Fahey, D. W., and Lee, D. S., "Aviation and Climate Change: A Scientific Perspective," *Carbon & Climate Law Review*, Vol. 10, No. 2, 2016, pp. 97–104.

[12] Wilcox, L. J., Shine, K. P., and Hoskins, B. J., "Radiative forcing due to aviation water vapour emissions," *Atmospheric Environment*, Vol. 63, 2012, pp. 1–13. https://doi.org/10.1016/j.atmosenv.2012.08.072, URL http://dx.doi.org/10.1016/j.atmosenv.2012.08.072.

[13] Gauss, M., Isaken, I. S. A., Wong, S., and Wang, W. C., "Impact of H2O emissions from cryoplanes and kerosene aircraft on the atmosphere," *Journal of Geophysical Research: Atmospheres*, Vol. 108, No. 10, 2003, pp. 1–11. https://doi.org/10.1029/2002jd002623.

[14] Johansson, K. O., Head-Gordon, M. P., Schrader, P. E., Wilson, K. R., and Michelsen, H. A., "Resonance-stabilized hydrocarbon-radical chain reactions may explain soot inception and growth," *Science*, Vol. 361, No. 6406, 2018, pp. 997–1000. https://doi.org/10.1126/science.aat3417.

[15] Di Domenico, M., Gerlinger, P., and Aigner, M., "Development and validation of a new soot formation model for gas turbine combustor simulations," *Combustion and Flame*, Vol. 157, No. 2, 2010, pp. 246–258. https://doi.org/10.1016/j.combustflame.2009.10.015, URL http://dx.doi.org/10.1016/j.combustflame.2009.10.015.

[16] Omidvarborna, H., Kumar, A., and Kim, D. S., "Recent studies on soot modeling for diesel combustion," *Renewable and Sustainable Energy Reviews*, Vol. 48, 2015, pp. 635–647. https://doi.org/10.1016/j.rser.2015.04.019, URL http://dx.doi.org/10.1016/j.rser.2015.04.019.

[17] Steinbach, A., Dittmann, T., Gerlinger, P., Aigner, M., and Eggels, R., "Soot Prediction in an Aircraft Combustor at Realistic Operation Conditions," *Volume 4A: Combustion, Fuels, and Emissions*, 2018, p. 8. https://doi.org/10.1115/GT2018-75366, URL https://doi.org/10.1115/GT2018-75366, v04AT04A018.

[18] Burkhardt, U., Bock, L., and Bier, A., "Mitigating the contrail cirrus climate impact by reducing aircraft soot number emissions," *Climate and Atmospheric Science*, Vol. 1, 2018. https://doi.org/10.1038/s41612-018-0046-4, URL http://dx.doi.org/10.1038/s41612-018-0046-4.

[19] Baklacioglu, T., "Fuel flow-rate modelling of transport aircraft for the climb flight using genetic algorithms," *Aeronautical Journal*, Vol. 119, No. 1212, 2015, pp. 173–183. https://doi.org/10.1017/S0001924000010320.

[20] Lee, D. S., Pitari, G., Grewe, V., Gierens, K., Penner, J. E., Petzold, A., Prather, M. J., Schumann, U., Bais, A., Berntsen, T., Iachetti, D., Lim, L. L., and Sausen, R., "Transport impacts on atmosphere and climate: Aviation," *Atmospheric Environment*, Vol. 44, No. 37, 2010, pp. 4678–4734. https://doi.org/10.1016/j.atmosenv.2009.06.005, URL http://dx.doi.org/10.1016/j.atmosenv.2009.06.005.

[21] Chandrasekaran, N., and Guha, A., "Study of prediction methods for NOx emission from turbofan engines," *Journal of Propulsion and Power*, Vol. 28, No. 1, 2012, pp. 170–180. https://doi.org/10.2514/1.B34245.

[22] Ommi, F., and Azimi, M., "Most effective combustion technologies for reducing Nox emissions in aero gas turbines," *The International Journal of Multiphysics*, Vol. 6, No. 4, 2012, pp. 417–424. https://doi.org/10.1260/1750-9548.6.4.417.

[23] Gangoli Rao, A., Yin, F., and Van Buijtenen, J. P., "A hybrid engine concept for multi-fuel blended wing body," *Aircraft Engineering and Aerospace Technology*, Vol. 86, No. 6, 2014, pp. 483–493. https://doi.org/10.1108/AEAT-04-2014-0054.

[24] Grewe, V., Bock, L., Burkhardt, U., Dahlmann, K., Gierens, K., Hüttenhofer, L., Unterstrasser, S., Gangoli Rao, A., Bhat, A., Yin, F., Reichel, T. G., Paschereit, O., and Levy, Y., "Assessing the climate impact of the AHEAD multi-fuel blended wing body," *Meteorologische Zeitschrift*, Vol. 26, No. 6, 2017, pp. 711–725. https://doi.org/10.1127/metz/2016/0758.

[25] Abbot, D., Giannotta, A., Sun, X., Gauthier, P., and Sethi, V., "Thermoacoustic Behaviour of a Hydrogen Micromix Aviation Gas Turbine Combustor Under Typical Flight Conditions," *Volume 6: Ceramics and Ceramic Composites; Coal, Biomass, Hydrogen, and Alternative Fuels; Microturbines, Turbochargers, and Small Turbomachines*, 2021, p. 12. https://doi.org/10.1115/GT2021-59844, URL https://doi.org/10.1115/GT2021-59844, v006T03A013.

[26] Köhler, M. O., Rädel, G., Shine, K. P., Rogers, H. L., and Pyle, J. A., "Latitudinal variation of the effect of aviation NOx emissions on atmospheric ozone and methane and related climate metrics," *Atmospheric Environment*, Vol. 64, No. x, 2013, pp. 1–9. https://doi.org/10.1016/j.atmosenv.2012.09.013, URL http://dx.doi.org/10.1016/j.atmosenv.2012.09.013.

[27] Gierens, K., Kärcher, B., Mannstein, H., and Mayer, B., "Aerodynamic contrails: Phenomenology and flow physics," *Journal of the Atmospheric Sciences*, Vol. 66, No. 2, 2009, pp. 217–226. https://doi.org/10.1175/2008JAS2767.1.

[28] Whelan, G. M., Cawkwell, F., and Mannstein, H., "The use of Meteorological Data to Improve Contrail Detection in Thermal Imagery over Ireland." *Remote Sensing and Photogrammetry Society Annual Conference 2009*, 2017, pp. 8–11.

[29] Schumann, U., "On Conditions for Contrail Formation from Aircraft Exhausts," *Meteorol. Zeitschrift*, 1996, pp. 4–23.

[30] Djojodihardjo, H., "Space Monitoring of Cirrus Clouds and Contrails for Climate Change Correction and Control," *IAA Climate Change and Disaster Management Conference, Mexico City*, Vol. September 2015, 2015, p. 20.

[31] Iwabuchi, H., Yang, P., Liou, K. N., and Minnis, P., "Physical and optical properties of persistent contrails: Climatology and interpretation," *Journal of Geophysical Research Atmospheres*, Vol. 117, No. 6, 2012, pp. 1–18. https://doi.org/10.1029/2011JD017020.

[32] Gorbunov, B., Baklanov, A., Kakutkina, N., Windsor, H. L., and Toumi, R., "Ice nucleation on soot particles," *Journal of Aerosol Science*, Vol. 32, No. 2, 2001, pp. 199–215. https://doi.org/10.1016/S0021-8502(00)00077-X.

[33] Ström, L., and Gierens, K., "First simulations of cryoplane contrails," *Journal of Geophysical Research Atmospheres*, Vol. 107, No. 18, 2002, pp. AAC 2–1–AAC 2–13. https://doi.org/10.1029/2001JD000838.

[34] Köhler, M. O., Rädel, G., Dessens, O., Shine, K. P., Rogers, H. L., Wild, O., and Pyle, J. A., "Impact of perturbations to nitrogen oxide emissions from global aviation," *Journal of Geophysical Research Atmospheres*, Vol. 113, No. 11, 2008. https://doi.org/10.1029/2007JD009140.

[35] Thatcher, D. R., and Jablonowski, C., "A moist aquaplanet variant of the Held-Suarez test for atmospheric model dynamical cores," *Geoscientific Model Development*, Vol. 9, No. 4, 2016, pp. 1263–1292. https://doi.org/10.5194/gmd-9-1263-2016.

[36] Hoffmann, P., *The Forever Fuel: The Story of Hydrogen*, 1st ed., Routledge, 1981. https://doi.org/10.4324/9780429311000.

[37] Hoffmann, P., *Tomorrow's Energy: Hydrogen, Fuel Cells, and the Prospects for a Cleaner Planet*, 1st ed., The MIT Press, 2001.

[38] Kahraman, N., Tangöz, S., and Akansu, S. O., "Numerical analysis of a gas turbine combustor fueled by hydrogen in comparison with jet-A fuel," *Fuel*, Vol. 217, No. August 2017, 2018, pp. 66–77. https://doi.org/10.1016/j.fuel.2017.12.071.

[39] Carter, R., "Development Of A Liquid Hydrogen Combustion High Bypass Turbofan Model In NPSS," *Mechanical Engineering and Materials Science Independent Study*, 2021.

[40] Sorokin, A., Arnold, F., and Wiedner, D., "Formation and growth of sulfuric acid-water cluster ions: Experiments, modelling, and implications for ion-induced aerosol formation," *Atmospheric Environment*, Vol. 40, No. 11, 2006, pp. 2030–2045. https://doi.org/10.1016/j.atmosenv.2005.11.053.

[41] Derakhshandeh, P., Ahmadi, A., and Dashti, R., "Simulation and technical economic environmental optimization of the General Electric GE90 hydrogen turbofan engine," *International Journal of Hydrogen Energy*, Vol. 46, No. 5, 2021, pp. 3303–3318. https://doi.org/10.1016/j.ijhydene.2020.10.182, URL https://doi.org/10.1016/j.ijhydene.2020.10.182.

[42] Yahya, M. Z. W., Azami, M. H., Savill, M., Li, Y. G., Khan, S. A., and Warimani, M. S., "Modelling of a three-shaft high-bypass-ratio engine performance and emission prediction using hydrogen fuels," *International Journal of Innovative Technology and Exploring Engineering*, Vol. 8, No. 6, 2019, pp. 484–490.

[43] Boretti, A., "Testing the hypothesis hydrogen jets may significantly contribute to global warming through jets contrails," *International Journal of Hydrogen Energy*, Vol. 46, No. 73, 2021, pp. 36610–36618. https://doi.org/10.1016/j.ijhydene.2021.08.173, URL https://doi.org/10.1016/j.ijhydene.2021.08.173.

[44] Samset, B. H., Myhre, G., Schulz, M., Balkanski, Y., Bauer, S., Berntsen, T. K., Bian, H., Bellouin, N., Diehl, T., Easter, R. C., Ghan, S. J., Iversen, T., Kinne, S., Kirkeväg, A., Lamarque, J. F., Lin, G., Liu, X., Penner, J. E., Seland, O., Skeie, R. B., Stier, P., Takemura, T., Tsigaridis, K., and Zhang, K., "Black carbon vertical profiles strongly affect its radiative forcing uncertainty," *Atmospheric Chemistry and Physics*, Vol. 13, 2013, pp. 2423–2434. https://doi.org/10.5194/acp-13-2423-2013.

[45] Marquart, S., Ponater, M., Strom, L., and Gierens, K., "An upgraded estimate of the radiative forcing of cryoplane contrails," *Meteorologische Zeitschrift*, Vol. 14, No. 4, 2005, pp. 573–582. https://doi.org/10.1127/0941-2948/2005/0057.

[46] Eurocontrol, "User Manual for the Base of Aircraft Data (BADA)," *European Organisation for the Safety of Air Navigation, Eurocontrol*, Vol. 3.6, 2004, p. 1. URL https://www.eurocontrol.int/publication/user-manual-base-aircraft-data-bada.

[47] Proesmans, P.-J., and Vos, R., "Airplane Design Optimization for Minimal Global Warming Impact," *Journal of Aircraft*, Vol. 59, No. 5, 2022, pp. 1363–1381. https://doi.org/10.2514/1.C036529.

[48] Planès, T., Delbecq, S., Pommier-Budinger, V., and Bénard, E., "Simulation and evaluation of sustainable climate trajectories for aviation," *Journal of Environmental Management*, Vol. 295, 2021. https://doi.org/10.1016/j.jenvman.2021.113079.

[49] Meinshausen, M., Raper, S. C. B., and Wigley, T. M. L., "Emulating coupled atmosphere-ocean and carbon cycle models with a simpler model, MAGICC6 - Part 1: Model description and calibration," *Atmospheric Chemistry and Physics*, Vol. 11, No. 4, 2011, pp. 1417–1456. https://doi.org/10.5194/acp-11-1417-2011.

[50] Lim, L., and Lee, D. S., "Quantifying the effects of aviation on radiative forcing and temperature with a climate response model," *Proceedings of the TAC-Conference*, 2006, pp. 202–207.

[51] Grewe, V., Gangoli Rao, A., Grönstedt, T., Xisto, C., Linke, F., Melkert, J., Middel, J., Ohlenforst, B., Blakey, S., Christie, S., Matthes, S., and Dahlmann, K., "Evaluating the climate impact of aviation emission scenarios towards the Paris agreement including COVID-19 effects," *Nature Communications*, Vol. 12, No. 1, 2021, pp. 1–10. https://doi.org/10.1038/s41467-021-24091-y, URL http://dx.doi.org/10.1038/s41467-021-24091-y.

[52] Ruijgrok, G., *Elements of Airplane Performance*, Delft Academic Press, 2009.

[53] Cuesta, M., *Motores de Reacción: Tecnología y operación de vuelo*, Paraninfo, 1986.

[54] Baughcum, S., *Scheduled Civil Aircraft Emission Inventories for 1992: Database Development and Analysis*, NASA contractor report, NASA, Langley Research Center, 1996. URL https://books.google.es/books?id=D3tUugEACAAJ.

[55] Turgut, E. T., and Usanmaz, O., "An assessment of cruise NOx emissions of short-haul commercial flights," *Atmospheric Environment*, Vol. 171, 2017, pp. 191–204. https://doi.org/10.1016/j.atmosenv.2017.10.013.

Appendix

A. Fleet Design Parameters

The fleet is composed of several aircraft, Table 10 displays the different aircraft analysed in the study and the inputs for the program.

Table 10   Characteristics of the aircraft investigated in the study.

Characteristics	FZM1G	B767S
Fuel Type	hydrogen	kerosene
Cruise Altitude [km]	10.7	10.0
MTOW [kg]	150 800	170 000
OEW [kg]	104 800	96 500
Design Range [km]	10 650	10 650
Design Payload [kg]	29 250	29 250
Design Fuel [kg]	16 750	44 250
S_{ref} [m^2]	245	255
Span [m]	52.0	52.0
Wing Loading [kg/m^2]	616	667
CL/CD [-]	19.9	22.1
$C_{D,0}$ [-]	0.012	0.010
k [-]	0.052	0.050

B. EINOx Computation

Boeing fuel flow method 2 [54] was selected for the computation of EINO$_x$ and Eq. (6) is used to calculate the final emitted NO$_x$. The equation includes the fuel flow of the engine ($\dot{m}_{\text{eng}}$), time (t) and the number of engines (N_{eng}).

$$NO_x = EINO_{x,\text{Alt}} \, \dot{m}_{\text{eng}} \, t \, N_{\text{eng}} \tag{6}$$

EINO$_{x,\text{Alt}}$ at the flight altitude can be calculated using Eq. (7), where EINO$_{x,\text{SL}}$ (at sea level) and the dimensionless coefficients θ_{amb} and δ_{amb} are used.

$$EINO_{x,\text{Alt}} = EINO_{x,\text{SL}} \left(\frac{\delta_{\text{amb}}^{1.02}}{\theta_{\text{amb}}^{3.3}} \right)^{0.5} e^I \tag{7}$$

The dimensionless coefficients represent the relative temperature and pressure with respect to sea level conditions.

$$\theta_{\text{amb}} = \frac{T_{\text{amb}}}{288.15} \tag{8} \qquad\qquad \delta_{\text{amb}} = \frac{P_{\text{amb}}}{1013} \tag{9}$$

Moreover, EINO$_{x,\text{SL}}$ can be calculated using the relation proposed by Turgut and Usanmaz [55], please note that Eq. (10) is exclusively used for kerosene fuel, as it is extracted from kerosene combustion engines. $\dot{m}_{\text{SL}}$ can be calculated using Eq. (11).

$$EINO_{x,\text{SL}} = 18.924\dot{m}_{\text{SL}} + 0.763 \tag{10}$$

$$\dot{m}_{\text{SL}} = \dot{m}_{\text{Alt}} \frac{\theta_{\text{amb}}^{3.8}}{\delta_{\text{amb}}} e^{0.2M^2} \tag{11}$$

In Eq. (11), M is the Mach number, and $\dot{m}_{Alt}$ is the calculated fuel flow at the flight altitude given by the engine model. Please note that the different cruise speeds of the aircraft to be analyzed in the study will cause a deviation on the NO$_x$ emitted. e^I represents the humidity factor correction. For that, Eq. (12) with altitude h was used.

$$I = 19 \left(0.00634 - 10^{-3}\, e^{-0.0001426\,(h-12900)} \right) \tag{12}$$